Combustion and Flame 166 (2016) 34–44

Contents lists available at ScienceDirect

Combustion and Flame

journal homepage: www.elsevier.com/locate/combustflame

Droplet burning rate enhancement of ethanol with the addition of graphite nanoparticles: Influence of radiation absorption

Saad Tanvir, Li Qiao*

School of Aeronautics and Astronautics, Purdue University, West Lafayette, IN 47907, USA

ARTICLE INFO

Article history:
Received 29 May 2015
Revised 21 December 2015
Accepted 21 December 2015
Available online 29 January 2016

Keywords:
Nanofluid
Droplet stream combustion
Burning rate enhancement
Radiation absorption
Monte Carlo

ABSTRACT

A droplet stream flame was used to measure the burning rate of ethanol droplets with the addition of graphite nanoparticles. Two particle sizes, 50 nm and 100 nm, were used for this study. Results indicate that as particle concentration is increased, the burning rate of the resulting nanofluid droplet also increases. The maximum enhancement of 62% was observed with the addition of 3 wt.% 50 nm graphite nanoparticles. To understand the burning-rate-enhancement phenomenon, a model was developed to estimate the radiation absorptivity by the hybrid droplet from the stream flame. The computational models determine the ratio of radiation retention by the entire depth of the fluid (volumetric absorptivity) using optical properties of both the particles and the fluid along with the penetration of radiation within the nanofluid using the well-known Monte Carlo algorithm that incorporates the aforementioned calculated optical properties of the nanofluid. Results indicate that radiation absorption by the hybrid droplet does play a role in the enhancement of burning rate. More importantly, the absorption is not uniform within the hybrid droplet. It is localized in the region near the droplet surface, promoting boiling at the droplet surface. This mechanism is believed to be responsible for the observed increased burning rate.

1. Introduction

Nanofluid fuels can be defined as liquid fuels with stable suspension of nanometer-sized particles. Energetic nanoparticles such as aluminum (Al) and boron (B) have high combustion energies and have been used as additives in propellants [1–4]. Research in the past decade has shown that when either energetic or catalytic nanoparticles, are mixed with traditional liquid fuels, it can be advantageous in propulsion applications, e.g., enhanced ignition probability [5], reduction in ignition delay [6,7], as well as reduced ignition temperature [3,4,8,9].

Sabourin et al. [10–12] investigated the burning characteristics of monopropellants consisting of liquid nitromethane and nanoparticles of graphene, and silicon- and aluminum-based oxides. The results show that a small addition of nanomaterials results in a substantial increase in burning rate. This is attributed to the nanoparticles having a significantly large surface area which increases the rate of nitromethane decomposition. McCown et al. [13] later explored the effect of adding higher energy density metallic nanoparticles such as Al on the burning rate of nitromethane and found 5 wt.% addition of Al resulted in a burning rate increase by 71–300% depending on the operating pressure. However, the mechanism was not clear. Several mechanisms could potentially explain the burning rate enhancement phenomenon as a result of particle addition, e.g., reduction in surface tension and surface energy at the liquid/gas interface, radiation absorption of nanoparticles, and a physical interaction between the particles and ethanol (wetting) increasing the interface area between the gas and liquid phases. It was not clear which mechanism was dominant. It was hypothesized that enhanced heat transport through radiation absorption and emission by the nanoparticles was one of the mechanisms responsible for this behavior.

Nanofluid combustion is an extremely complex phenomenon. Since the nanofluid fuel contains both liquid and nano-sized solid particles, the combustion process becomes multi-phase, multi-component and multi-scale. During the combustion of nanofluid fuels, it is expected that multiple simultaneous processes take place: liquid fuel vaporization, combustion of that liquid fuel in the gaseous phase, burning of the solid nanoparticles, mass and energy transfer between the three phases, and dynamics of the particles. In most studies of droplet combustion, radiation absorption by the droplet is usually neglected. This is because most liquid fuels are nearly transparent to the radiation emission from a flame. This, however, may not be true for a nanofluid droplet. It was hypothesized that the absorption of radiation by the nanoparticles within the droplet may enhance burning.

* Corresponding author. Fax: +1 765 494 0307.
E-mail address: lqiao@purdue.edu (L. Qiao).

http://dx.doi.org/10.1016/j.combustflame.2015.12.021
0010-2180/

Motivated by this, the current authors studied the effect of nano-Al addition on the burning rate of ethanol [14]. Results indicated that a small amount of addition of Al nanoparticles significantly enhanced droplet burning rate. For example, with 5 wt.% addition of Al nanoparticles in ethanol, the droplet burning rate increased by 140%. It was also observed that droplet size had little effect on burning rate. A simple model was developed to estimate the absorption of radiation energy emitted from the flame by the nanoparticles, which may be responsible for burning rate enhancement as more energy is available for evaporation. Results showed that absorption of radiation energy by the nanoparticles indeed plays an important role in energy transfer and cannot be neglected. However, this model adopted several assumptions. It considered radiation absorption by nanoparticles only and neglected the complex interactions between radiation waves and the two-phase media in the droplet. The predicted enhancement in radiation energy absorption as a function of particle concentration did not however correlate well with the measured burning rates for the smaller droplet size but showed good agreement with the burning rate of the larger droplet size. Nevertheless, a better model is required to quantitatively understand the radiation absorption behavior of nanofluid type fuels.

The current study reports experimentally obtained data on the burning rate variation of graphite based nanofluid fuels and explains how the optical properties of graphite at the nanoscale affect the radiation absorption of incoming infrared radiation. This is done to get insight as to how the radiation is absorbed and then distributed within the nanofluid droplet and whether the addition of graphite has significant impact on the absorption behavior of ethanol. Graphite was chosen mainly because its reflective index, especially at nanoscale, is better defined than the other nanoparticles such as aluminum, which helped to improve the accuracy of the models. Furthermore, a number of researchers have studied the combustion characteristics of liquid hydrocarbon fuels mixed with carbon particles [15–18]. The motivation was to utilize cheap and abundant coal to enhance energy security and burning of liquid fuels. Ethanol was chosen because it is a polar fuel. As a result, the nanofluid fuels exhibit good suspension quality even without the use of a surfactant, which, otherwise, would complicate the analysis. A droplet stream experiment [14] was used to determine the burning rate of ethanol with the addition of graphite nanoparticles. Both SEM (scanning electron microscopy) of the burnt graphite samples and a time scale analysis (droplet evaporation time scale vs. particle aggregation time scale) indicate that aggregation does occur. However, its severity is not to the extent predicted in literature due to the small timescales involved in the current work.

The goal of our computational models is one to determine the ratio of radiation retention by the entire depth of the fluid (volumetric absorptivity) using optical properties of both the particles and the fluid, and second to determine the penetration of radiation within the nanofluid using the well-known Monte Carlo algorithm that incorporates the optical properties of the nanofluid.

The first model utilizes optical properties of graphite nanoparticle and ethanol as well as Mie theory to determine the volumetric absorptivity of the resulting nanofluid. Note the volumetric absorptivity is a “property” of the fluid, which does not reflect the dynamic process of light absorption, scattering and extinction spatially in a nanofluid. It simply gives an idea how much radiation energy can be absorbed by the two-phase fluid and how much radiation energy can penetrate. The method to determine volumetric absorptivity is commonly used in nanofluids research regarding their radiation properties for various applications [19–23]. Researchers have shown that even a small amount of nanoparticle addition (less that 1 wt.%) can result in a near complete absorption of incoming radiation [21]. Assuming that nanoparticles are evenly distributed within the nanofluid, the optical properties of the nanofluid remain constant at all depths from the surface. Our group previously measured the transmission spectrum of several nanofluids [24]; the results show that the computed extinction (absorption and scattering) coefficients by treating the nanofluid as a whole entity (using volume fraction or number density) gave comparable results to the measured data.

It is also believed that the incoming radiation is not uniform within the nanofluid due to the extinction by the nanoparticles which have encountered radiation. This is the reason we carried out Monte Carlo simulation to determine the spatial distribution of the absorbed radiation with in the nanofluid. The Monte Carlo technique, based on the random walks that photons make as they travel through a medium, simulates light propagation in the medium. The results show that most of the radiation energy from the flame is localized to and absorbed by the nanoparticles closest to the gas/liquid surface. This means that the nanoparticles near the droplet surface absorbed most of the incoming radiation energy and little was left for the particles near the center of the droplet. We believe the localized boiling at and near the surface of the droplet promote faster vaporization of liquid ethanol and is mainly responsible for droplet burning rate increase.

2. Experimental methods

2.1. Fuel preparation and characterization

The preparation of fuel mixtures requires special care to achieve homogeneous, stable, long-term suspension and a low level of particle agglomeration. Studies have shown that sonication along with the addition of surfactants have the capacity to reduce the agglomeration of nanoparticles in nanofluids. Homogeneity of nanoparticles with in a nanofluid is one of the major barriers holding this fuel to be used in real world applications. However, it is our effort to maximize the stability of nanofluids through various experimental methods. Physical methods such as sonication delay aggregation. Such ultrasonic-induced disruption in liquids is well known [25].

The nanofluid fuels are prepared using physical dispersion methodologies as discussed in the earlier studies [26,27]. The appropriate amounts of particles were first vigorously stirred with the base fuel. This was followed by sonication of the colloidal mixture in an ultrasonic disrupter (QSonica Q500A) to minimize and delay particle agglomeration. The sonication was performed in an ice bath to maintain a constant temperature of the nanofluid. The sonicator generates a series of 4 s long pulses with 4 s spacing. The mixture was sonicated for a duration of 8 min.

Ethanol was used as a base fuel for the current study. Graphite nanoparticles (averaged size of 50 nm and 100 nm) were considered as additives to ethanol. The amount of particles added was measured using an analytical scale (Torban AGZN 100) with an accuracy of 0.1 mg. Nanofluid samples prepared (1–3 wt.% graphite in ethanol) maintained good suspension quality without the presence of a surfactant.

Dynamic Light Scattering technique was used to examine the effect of sonication time on the long-term stability of nanofluids. The results show that nanofluid stability increases with increasing sonication time. However, as time after sonication increases, the nanoparticles begin to aggregate therefore increasing the average particle size within the nanofluid. As a result, the samples were sonicated for a sufficiently-long time. Additionally, the experiment was performed immediately after sonication. The equipment was thoroughly cleaned and rinsed before each test to minimize deposition of layers of nanoparticles within the tubing as well as within the droplet generation system. Based on the precautions taken during the course of the experiment, we assume that the nanoparticles were evenly distributed within the droplets.

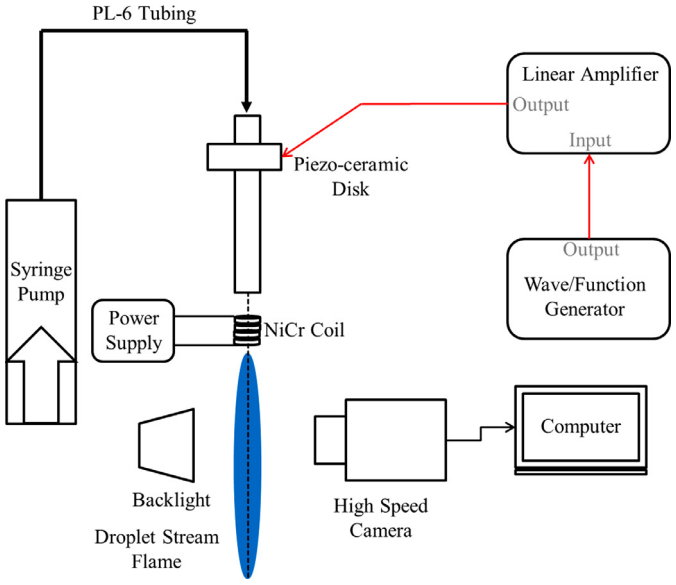

Fig. 1. Schematic of the droplet steam combustion experiment.

Furthermore, droplet size has little impact on the distribution of nanoparticles within the fluid.

2.2. Experimental setup – droplet stream flame

A NiCr heating coil attached to a high voltage power supply was used to ignite the droplet stream. The setup (Fig. 1), similar to the one described earlier in ref. [14], consists of a vibrating orifice droplet generator, a dual-syringe mechanical syringe pump system (KD Scientific Legato 200), a wave function generator, a linear amplifier, and a high speed camera along with a backlight. As the fluid passes through the droplet generator, the square wave signal causes the piezoceramic disk within the droplet generator to oscillate and inflict longitudinal disturbances to the fluid jet, thus perturbing the fluid. In accordance with the Rayleigh Instability theory, the fluid, when disturbed at the proper frequency, will break-up from a uniform jet stream into a uniform stream of equally sized and spaced spherical droplets. The heating coil was placed at a distance of 20 mm downstream of the orifice. This was set to avoid upstream propagation of the droplet stream flame. Droplet burning rate was determined by measuring droplet sizes at periodic locations downstream of the ignition coil using backlight shadowgraphy technique using a phantom V7.3 high-speed camera. The measurements of droplet sizes were taken only in regions where the droplet stream was uniform and stable. A DSLR (digital single-lens reflex) camera was used to capture the burning behavior of the stream. A protective screen was placed around the flame to get better imaging and to isolate the flame from external air disturbances.

3. Results and discussion

3.1. Flame appearance and combustion residue analysis

Flame tests were conducted for pure ethanol and ethanol with up to 3 wt.% graphite nanoparticles. Two droplet sizes were considered: 200 and 410 μm. The stream combustion process can be divided into two distinctive stages. Stage I comprises of pure ethanol combustion, indicated by the region of a blue ethanol flame. In this stage, the droplets within the stream were uniformly distributed and undisturbed. Their size continues to regress steadily as they fall. Stage II is characterized by simultaneous combustion of both ethanol and graphite nanoparticles. This is evident from the appearance of flares in the flame zone surrounded by the blue ethanol flame. The graphite particles (and particle aggregates) are ejected from the droplets and brought to the droplet stream flame zone to burn resulting in many local particle flames. This integrated burning behavior is similar to what was observed in previous work [14,26,27]. Furthermore, in this stage the droplets inside the stream are no longer of uniform size and shape nor at a constant distance from each other.

Figure 2(a) and (b) shows the SEM images of the burned 50 nm and 100 nm graphite particles and their aggregates respectively collected downstream of the of the respective flames when 3 wt.% of particles were added to ethanol. As the particle size increases, the density and size of the combustion residues also increases. For all cases, however, the size of the residues (less than 5 μm) is still an order of magnitude smaller than the size of the nanofluid droplet (200 μm, 400 μm). This indicates that during the droplet burning process, particles within the droplet did not have enough time to form significantly large aggregates. However, the fact remains that the average size of the burned aggregates is on the order of 10 times bigger than the original size of the particles, so aggregation is important during the combustion process.

It is also fair to assume that the aggregation may start even before the flame is lit. However, limitations (mainly spatial) in diagnostic techniques prevent us from monitoring aggregation within the falling droplets.

3.2. Time scale analysis

We have concluded that aggregation had less impact on the burning process of smaller droplets. This was based on the fact that the burnt aggregates collected from the flame front had sizes an order of magnitude smaller than that of the droplet. This was however different from the observations made by Gan et al. [26,27] while examining millimeter sized droplets observed that aggregation played an important role in the burning process that even hindered burning rate. They found that the size of the aggregates was on the same order of magnitude as the droplet.

Motivated by this, we compared the characteristics time scales of droplet evaporation and particle aggregation. Such comparison would help to determine whether aggregation is an important process during droplet evaporation. The aggregation of nanoparticles is traditionally described by a dimensionless number C_R which is defined as the ratio of particle migration time (τ_{part}) to the droplet vaporization time (τ_{evap}) [28]. A large value of C_R indicates that particle migration is slow with a large τ_{part}, or the evaporation occurs quickly with a small τ_{evap}.

The particle migration time (τ_{part}) is the time required for two adjacent particles to assemble and is formulated as [28]

$$\tau_{part} = \frac{\bar{L}_m^2}{2D_p} \tag{1}$$

where the average distance between two adjacent particles is $\overline{L_m} = (V_d/n)^{1/3}$, V_d is the volume of a single droplet and n is the number of nanoparticles contained in the droplet. The diffusion coefficient of particles D_p is $k_BT/6\pi\eta r$, where k_B is the Boltzmann constant, T is the temperature of the droplet, η is the viscosity of the nanofluid and r is the radius of the moving sphere (nanoparticle).

The evaporation time scale indicates how fast the droplet is vaporizing. However, we did not use the 'total' time for the droplet to vaporize completely. Rather, the evaporation (or burning) timescale τ_{evap} is defined as the time of measurement for a droplet to reach the minimum measured droplet diameter during the experiment. It represents the total time of measurement of droplet regression (shown in Figs. 4 and 5). This was chosen to get an estimate of the

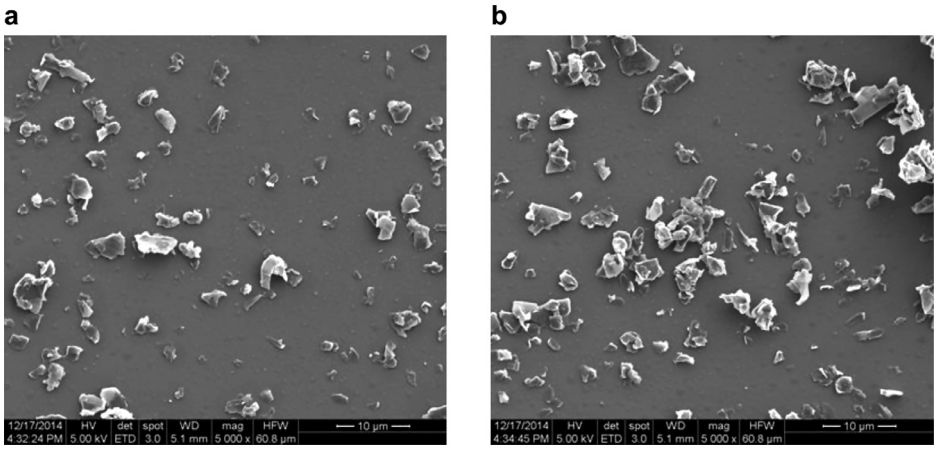

Fig. 2. SEM images of combustion residues of burned graphite particles and aggregates: (a) 3 wt.% 50 nm graphite and (b) 3 wt.% 100 nm graphite.

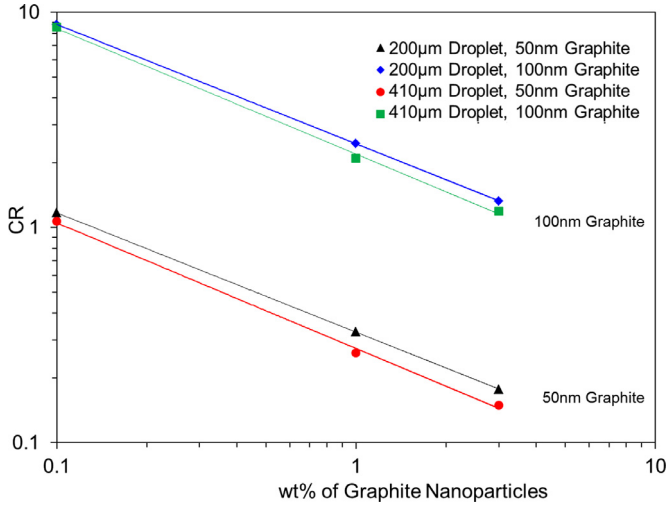

Fig. 3. C_R plotted as a function of particle size and concentration, and droplet size.

maximum degree of aggregation we can expect to see during the course of our measurements of droplet burning rate.

It is also noteworthy that only a small reduction in droplet diameter was considered for this particular study. Ideally, the evaporation time scale would correspond to the total vaporization time for all the ethanol to vaporize. Non-homogeneity of the droplet stream, however, prevented accurate droplet diameter measurement till complete vaporization. The time scale analysis was thus aimed to determine the aggregation times for the time duration of our experiment (accurately measuring the droplet diameter and determining burning rate). Hence the evaporation time was chosen to be the time at which the droplets reached their minimum measured diameter.

Figure 3 shows the variation of C_R as a function of particle concentration and droplet size. As the nanoparticle concentration increases, the value of C_R decreases. We know that burning rate increases with increasing particle concentration, thus τ_{evap} reduces. A decreasing C_R value with increasing particle concentration then indicates that the drop in τ_{part} is even bigger. This is because as particle concentration increases, the mean distance between two adjacent particles reduces, making particle collision and aggregation more frequent. In summary, as particle concentration increases the degree and rate of aggregation increases for all droplet sizes. It is also interesting to note that as droplet size reduces the C_R value slightly increases. This indicates that the vaporization time scales are smaller in smaller droplets. This effect however is not as significant.

The observed trend of C_R does strengthen the argument that increasing particle concentration increases aggregation intensity. The value of C_R reduces as a function of increasing particle concentration and decreasing particle size; showing that aggregation becomes increasingly important during the combustion process especially at higher particle concentrations and smaller particle sizes. This is because as particle size decreases the number density of particles within the droplet for the same mass loading rate increases. As the number density increases, the average distance between particles is reduced. This effect reduces the aggregation time scale and increases aggregation intensity within the nanofluid.

3.3. Effect of particle addition on droplet burning rate

Droplet burning rate was determined by measuring droplet sizes at periodic locations downstream of the ignition coil using backlight shadowgraphy technique. As described earlier, at a certain distance downstream of the ignition coil, particles and particle aggregates started to escape from the droplets and to burn. As a result, the stream was disrupted and could no longer remain stable and uniform. Thus, the measurements of droplet sizes were taken only in regions where the droplet stream was uniform and stable.

The initial droplet diameter (D_0) is defined as the droplet diameter at the exit of the heating coil. It is the point at which the stream flame begins. Indeed the heat from the flame causes the droplets originating from the orifice to begin vaporizing. However, due to the very small time scale between the exit of the orifice and the end of the heating coil, the difference in diameter of droplets was negligible. Therefore, we begin measuring the droplet diameters at the point where the flame starts.

Figures 4 and 5 show the variation of droplet diameter squared as a function of time for graphite/ethanol droplets (200 μm and 410 μm, respectively). Starting with 12.5 mm downstream from the end of the ignition coil, the measurements were taken in increments of 12.5 mm downstream of the flame. It was observed that the squared droplet size decreases linearly with time for pure ethanol and approximately for all graphite/ethanol fuels considered for this study, following the classical D^2-law.

Figure 6 shows the enhancement in burning rate of graphite based nanofluid fuels normalized to the burning rate of pure ethanol. The burning rate is determined by calculating the slope of the linear fits shown in Figs. 4 and 5. Clearly, the addition of nanoparticles results in an increase in burning rate of the resulting nanofluid. For example, for 3 wt.% addition of 50 nm graphite, the burning rate is enhanced by 58% for 200 μm droplets and 62% for 410 μm droplets. The enhancement however is less than what was observed for energetic Al based nanofluids where a 3 wt.% addition

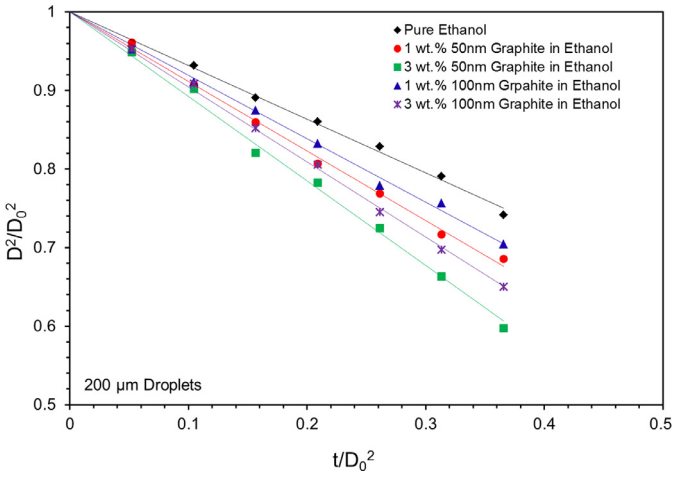

Fig. 4. Variation of droplet diameter squared as a function of time for 200 μm ethanol droplets with the addition of graphite nanoparticles.

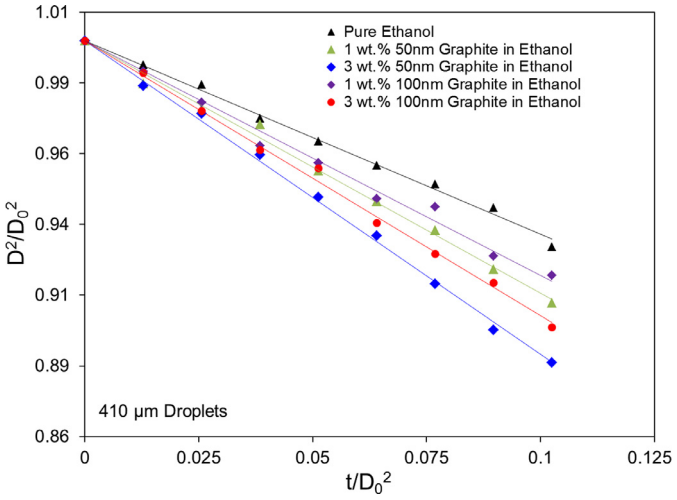

Fig. 5. Variation of droplet diameter squared as a function of time for 410 μm ethanol droplets with the addition of graphite nanoparticles.

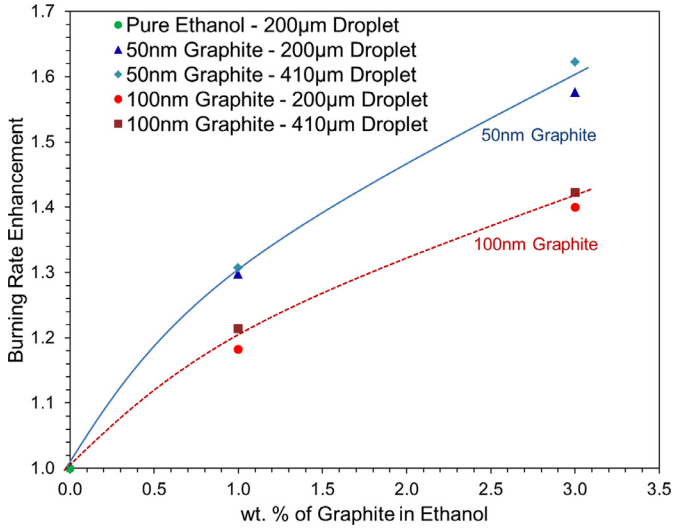

Fig. 6. Enhancement in burning rate as a function of particle concentration and size.

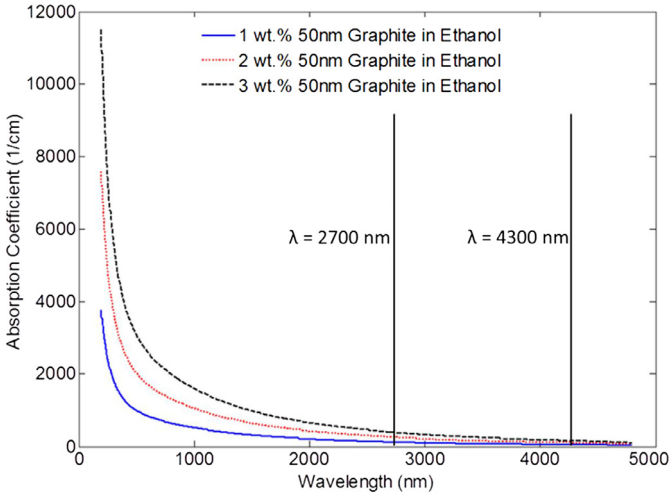

Fig. 7. Absorption coefficient of 50 nm graphite in ethanol nanofluid; 200 μm droplets.

resulted in a burning rate increase of 105% [14]. Lastly, with the reduction in particle size the burning rate increases further. This may be attributed to enhanced surface area for evaporation due to particle wetting at the liquid gas interface as earlier hypothesized by Sabourin et al. [10,11].

3.4. Optical properties of the nanofluid fuels

A primary goal of this study was to understand why burning rate increases and what factors determine the magnitude of increase based on nanoparticle type, size and concentration. We hypothesized that radiation absorption by the droplet from the stream flame plays an important role in burning rate enhancement. Motivated by this, our first step was to determine the optical properties of the hybrid fuel mixture. In this model, the optical properties of graphite [29], particle size (diameter, D) and droplet size are known parameters. Mie theory [30] was then used to determine the absorption coefficient of the particles as a function of wavelength (λ). Mie theory was used because the size parameter, $\alpha = \pi D/\lambda$, approaches unity for higher wavelengths making Rayleigh theory invalid. Considering the nanofluid as a cloud of uniform sized particles, the spectral absorption coefficient ($\sigma_{abs,\lambda}$) can be written as a function of absorption efficiency factor ($Q_{absorption}$) and N_T (number of particles per unit volume) as.

$$\sigma_{abs,\lambda} = \pi {R_p}^2 N_T Q_{absorption,\lambda} \tag{2}$$

where R_p is the radius of one nanoparticle. $Q_{absorption,\lambda}$ is a function of wavelength and is found using fundamentals of Mie theory that are well defined in [30]. Wavelengths (λ) ranging from 0.19 μm to 4.8 μm were considered. This range incorporates the visible and as well the infrared region of the emission spectrum. This was chosen to cover the two important bands of CO_2 radiation (at $\lambda = 2.7$ μm and 4.3 μm) and one important band of H_2O radiation ($\lambda = 2.7$ μm) emitted from the flame [31]. The term N_T introduces the effects of neighboring nanoparticles toward the absorption of incoming radiation. As particle concentration increases the number of particles per unit volume also increases therefore increasing the absorption coefficient.

Figures 7 and 8 show the absorption coefficients for 50 nm and 100 nm graphite nanoparticles in ethanol, respectively. Results indicate that as particle concentration increases the absorption coefficient also increases. This is due to presence of more particles per unit volume for higher concentrations. Furthermore, we also note that for lower wavelengths absorption coefficient also increases as a function of decreasing particle size. As particle size is

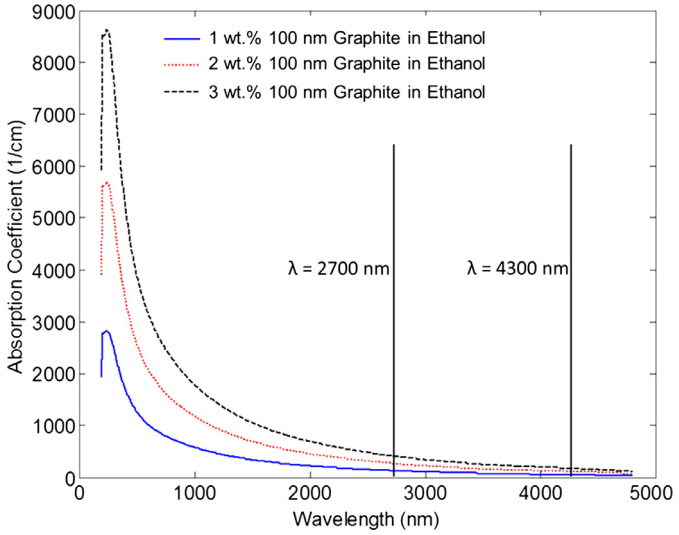

Fig. 8. Absorption coefficient of 100 nm graphite in ethanol nanofluid; 200 μm droplets.

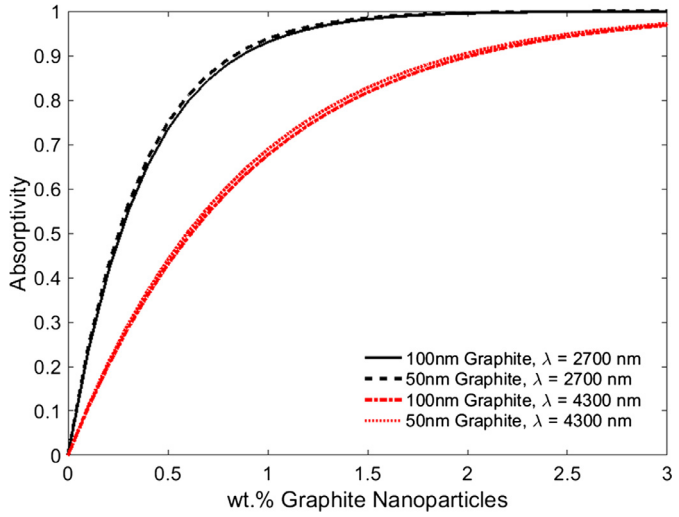

Fig. 9. Variation in absorptivity of 50 nm and 100 nm graphite in ethanol nanofluid (200 μm) as a function of particle concentration at wavelength of 2700 nm and 4300 nm.

reduced, the nanofluids contain more number of particles as compared to their larger counterparts for the same weight percentage. This increases the number of particles per unit volume and hence increases the absorption coefficient. However, as we enter into the infrared region, the effect diminishes and particle size has little impact on the absorption properties of the nanofluid. Lastly, the absorption coefficient is nearly independent of droplet size or medium depth.

Once we know the absorption coefficient of the nanofluid as a function of the incoming wavelength, the volumetric absorptivity (α_{np}) of the nanofluid can then be determined by using the Beer–Lambert relation [19,21,23] for the two important bands of radiation emitted from the ethanol flame (2700 nm and 4300 nm).

$$\alpha_{np} = \frac{I_{absorbed}}{I_{total}} = 1 - e^{-\sigma_{abs,\lambda} y} \tag{3}$$

where y is the depth of the nanofluid which can be approximated to be the diameter of the droplet and $\sigma_{abs,\lambda}$ is the absorption coefficient of the nanofluid at $\lambda = 2700$ nm and 4300 nm.

Figure 9 shows the volumetric absorptivity of 50 nm and 100 nm graphite in 200 μm ethanol nanofluid droplets as a function of particle concentration and particle size for $\lambda = 2700$ nm

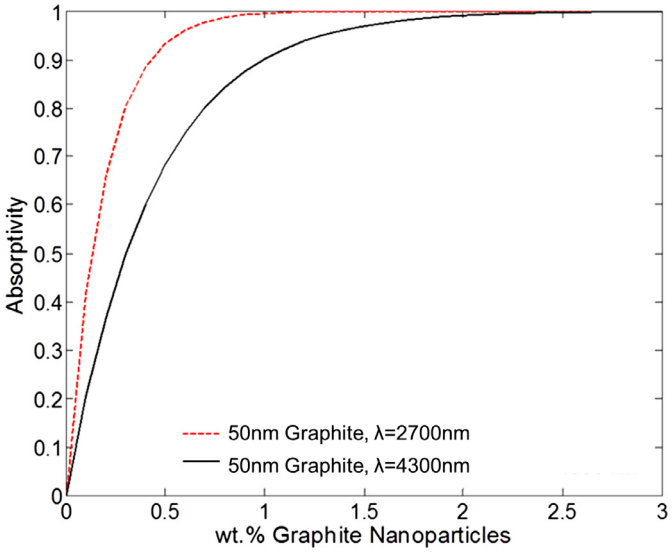

Fig. 10. Variation in absorptivity of 50 nm graphite in ethanol nanofluid as a function of particle concentration and wavelength of incoming radiation for 410 μm droplets.

and 4300 nm. We observe that as we increase particle concentration the absorptivity increases. This is because as particle concentration increases, the mean absorption coefficient of the nanofluid also increases. We notice that as nanoparticles are initially introduced to the fluid, the absorptivity rapidly increases to values close to 1 for low particle concentrations of graphite. This indicates that close to 100% of the incoming radiation is going to be absorbed by the nanofluid upon a small addition of graphite nanoparticles. This is significant since pure ethanol is almost completely transparent to incoming radiation. We therefore expect the total energy budget for droplet vaporization to increase significantly during the nanofluid droplet combustion process. We also observe that the effect of varying particle size has little impact on the absorptivity. However, the slightly higher absorptivity of 50 nm graphite nanofluids can be attributed to their higher number density as compared to 100 nm graphite particles for the same particle concentration. This leads to a higher number of particles per unit volume and therefore a higher absorptivity.

Another observation made from Fig. 9 is that as the wavelength increases from 2700 nm to 4300 nm, the absorptivity decreases for the same particle concentration. This effect is also visible in Fig. 10 for 410 μm droplets. The drop in absorptivity is due to the reduction in the absorption coefficient of graphite in ethanol nanofluid as we move deeper into the infrared regime.

Figures 11 and 12 highlight the effect of droplet size on the absorptivity of the nanofluid fuel. We see that as droplet size increases the absorptivity also increases upon nanoparticle addition. This is due to increase in penetration depth of the fluid. The increase in penetration depth allows for more total number of absorbing particles in the nanofluid for a certain particle concentration. This further reduces radiation transmission hence enhancing absorptivity.

The calculated absorptivity determines the amount of incoming radiation that is absorbed by the nanofluid droplet. The increase in the available energy (because of radiation absorption) for vaporization is expected to be one of the major factors that explain the increase in burning rate. From experimental results, we see that the burning rate increases rapidly for small nanoparticle concentrations (1 wt.%), after which the rate of increase is reduced. Modeling results of absorptivity show that for low particle concentrations, the graphite in ethanol nanofluids absorbs almost all of the incoming radiation. Hence, further increase in particle concentration does

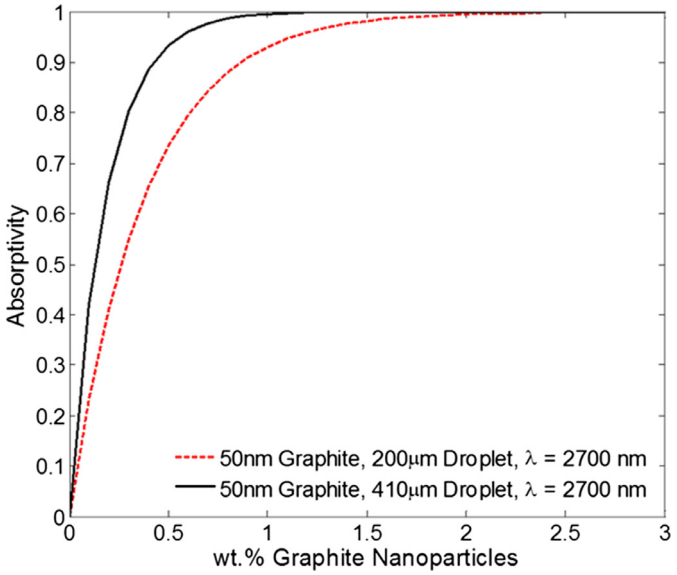

Fig. 11. Variation in absorptivity of 50 nm graphite in ethanol nanofluid as a function of particle concentration and droplet size at wavelength 2700 nm.

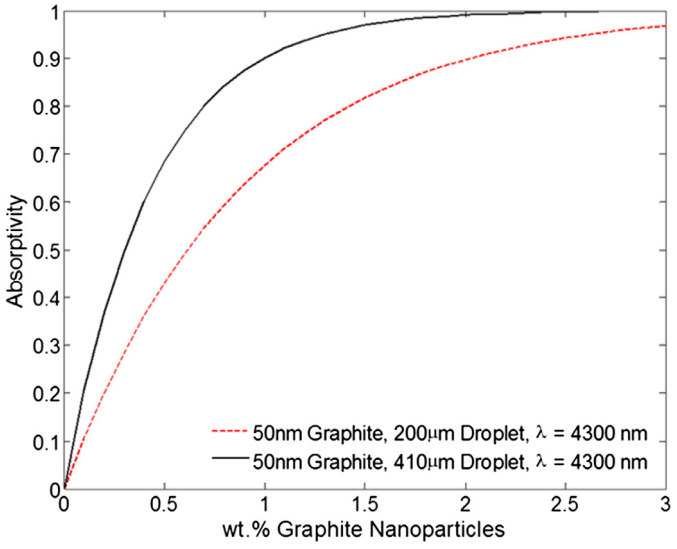

Fig. 12. Variation in absorptivity of 50 nm graphite in ethanol nanofluid as a function of particle concentration and droplet size at wavelength 4300 nm.

not affect the total energy budget. This results in a reduction in the rate of increase of burning rate as a function of particle concentration. It also indicates that mechanisms other than enhanced radiation absorption described briefly in the previous section become increasingly important at higher particle concentrations.

The significance of the results obtained with this particular model relates only to the amount of radiation retained by the nanofluid. Furthermore, in the regime of wavelength considered for this study, we see that the absorption coefficient is much greater than the scattering coefficient, which is why both absorption and extinction in the present results are very close to one other. This particular observation validates the use of incorporating Beer-Lambert law of volumetric absorptivity to estimate the radiation retention within the nanofluid [32].

3.5. Radiation penetration in a nanofluid droplet: Monte Carlo simulations

Literature [32] indicates that the absorption of radiation by nanofluids in not uniform. This means the portion of incoming radiation absorbed by the nanofluid (as determined in the previous section) is non-uniformly distributed within the fluid. With the increase of particle concentration, absorption becomes predominantly concentrated at the liquid–gas interface creating regions of elevated energy concentrations within the nanofluid [32]. To put this theory to the test, a standard Monte Carlo algorithm [33] was employed to monitor and track photon penetration into the nanofluid as a function of increasing particle concentration. The goal here is to see how the absorbed incoming radiation is distributed within the graphite–ethanol nanofluid.

Figure 13 shows the proposed geometry of the spherical droplet with incident infrared radiation. Section 3.4 already outlines the process to obtain nanofluid absorption coefficient based on Mie theory. Similarly, the spectral scattering coefficient ($\sigma_{sca,\lambda}$) can be written as a function of the scattering efficiency factor ($Q_{scattering}$) and N_T (number of particles per unit volume):

$$\sigma_{sca,\lambda} = \pi {R_p}^2 N_T Q_{scattering,\lambda} \tag{4}$$

where R_p is the radius of one nanoparticle. $Q_{scattering,\lambda}$ is a function of wavelength and is found using fundamentals of Mie theory that are well defined in [30,34]. To get an estimate of the radiation absorbed by the nanofluid from the ethanol flame, we only consider the two major bands of radiation emitted from the ethanol flame: $\lambda = 2.7$ μm (CO_2 and H_2O) and $\lambda = 4.3$ μm (CO_2).

The Monte Carlo routine begins with the launch of photons into the nanofluid. Here the initial photon position and trajectory are defined. It is assumed that a uniform collimated beam consisting of 10,000 photons is incident on the surface of the nanofluid. It is also assumed that the illumination is perpendicular to the *X*–*Y* plane and that the depth is specified by the penetration of each photon in the *Z*-direction into the droplet.

Once the photon is launched into the scattering nanofluid medium, it follows the *move* or *drift* step. Here the photon is moved a propagation distance Δs, which is a function of a random number, R_1, in the interval [0, 1] and the absorption and scattering coefficients of the nanofluid.

$$\Delta s = -\frac{\ln(R_1)}{\sigma_{abs} + \sigma_{sca}} \tag{5}$$

Monte Carlo routine estimates the mean free path between every scattering and absorption event to be $\frac{1}{\sigma_{abs}+\sigma_{sca}}$. Once the photon has propagated Δs, it is necessary to check whether the photon is still in the medium. Each propagation step of the photon is followed by a check to see if it has reached the boundary of the spherical droplet. This is done by determining the radial position of the photon and comparing it to the radial boundary of the nanofluid droplet. If the photon reaches the boundary of the nanofluid, it is either internally reflected back into the medium or it escapes the medium and is pronounced dead. The reflectivity of the nanofluid is calculated based on the optical properties of the nanofluid and surrounding air using Fresnel relations that are well known [30]. If the photon has not reached the boundary of the fluid or is reflected back into the medium, it will remain alive until it is completely absorbed by the fluid or escapes via the boundary.

In the present algorithm, the absorption of light by the nanofluid is tracked by assigning a weight, *W*, to the photon and updating it after every absorption step according to the nanofluid albedo [33]

$$albedo = \frac{\sigma_{sca}}{\sigma_{abs} + \sigma_{sca}} \tag{6}$$

where *albedo* and $1 - albedo$ are the fractional probability of being scattered and being absorbed, respectively. The weight of the photon is initially equal to 1. The weight is updated every absorption step till it reaches a threshold level after which the photon is declared dead or fully absorbed by the medium.

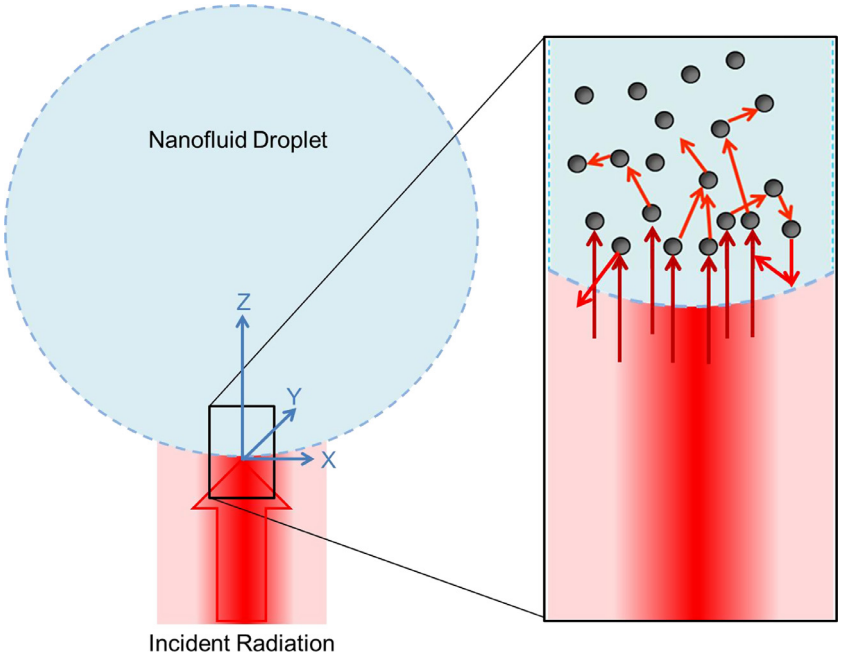

Fig. 13. Illustration of Monte Carlo simulations of photon penetration in a nanofluid.

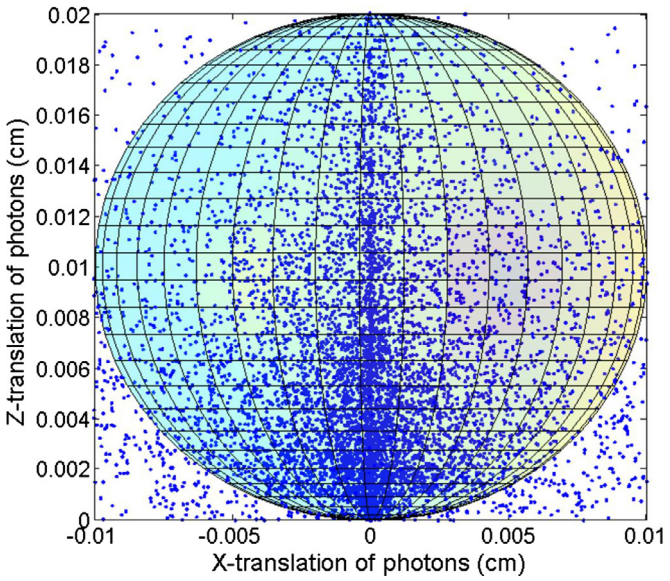

Fig. 14. Photon penetration into 1 wt.% 50 nm graphite in ethanol nanofluid droplet at $\lambda = 2700$ nm. The scatter represents final position of the photons inside the nanofluid (photons are incident at $Z = 0$).

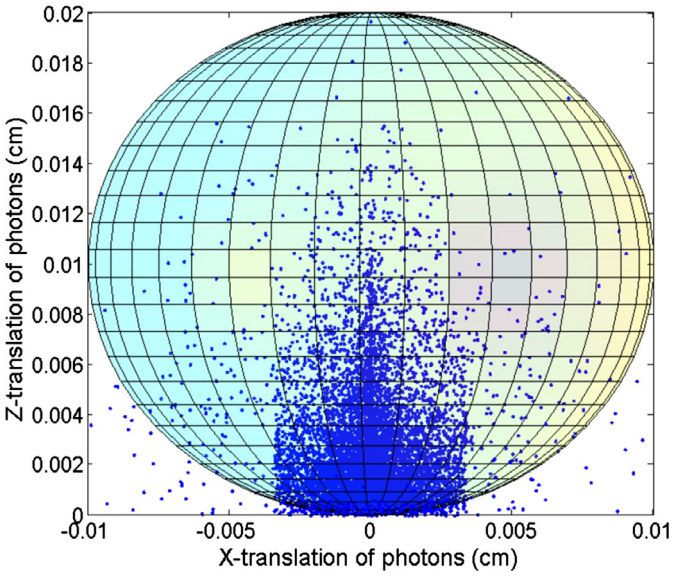

Fig. 15. Photon penetration into 3 wt.% 50 nm graphite in ethanol nanofluid droplet at $\lambda = 2700$ nm. The scatter represents final position of the photons inside the nanofluid.

The scattering of a photon is defined by the polar or scattering and azimuth angle with respect to the direction vector prior to scattering. In a standard Monte Carlo routine, the scattering angle is most commonly determined using the Henyey-Greenstein phase function [35] and the azimuth angle is chosen uniformly between 0 and 2π by assuming that scattering is isotropic [34]. The Monte Carlo routine allows the photon to scatter within the nanofluid till it either leaves the nanofluid boundary or is completely absorbed by the nanofluid.

Figures 14 and 15 show the results of photon tracking using the Monte Carlo routine for 50 nm graphite in ethanol nanofluids at a wavelength of 2700 nm. The scatter represents the final position of the photons inside the nanofluid droplet. In other words, the dots represent the position of each photon at the time of their respective deaths (fully absorbed by the fluid). The photons are incident on the surface of the nanofluid at $Z = 0$. Positive Z represents the depth inside the nanofluid. Results show that as particle concentration is increased, the penetration depth of the photons decreases. Meaning that most of the photons are absorbed closer to the nanofluid surface. This is due to the fact that the absorption coefficient of the nanofluids increases as a function of particle concentration for any given wavelength. This is clearly evident from Fig. 7. An increase in absorption coefficient reduces scattering probability and enhances absorption within the nanofluid.

Figures 16 and 17 show the results of photon tracking using for 50 nm graphite in ethanol nanofluids at a wavelength of 4300 nm. Similar observations are made. As particle concentration increases the penetration depth of photons decreases. Results here are consistent with those observed by Hogan et al. [32]. However, for the

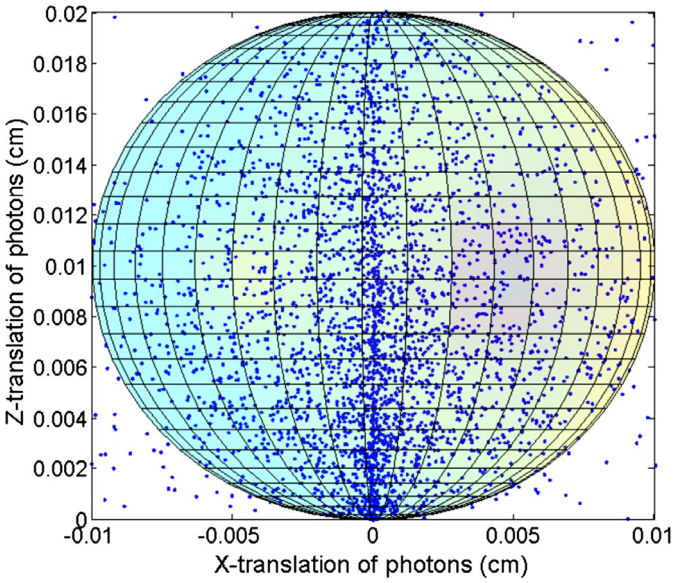

Fig. 16. Photon penetration into 1 wt.% 50 nm graphite in ethanol nanofluid droplet at $\lambda = 4300$ nm. The scatter represents final position of the photons inside the nanofluid.

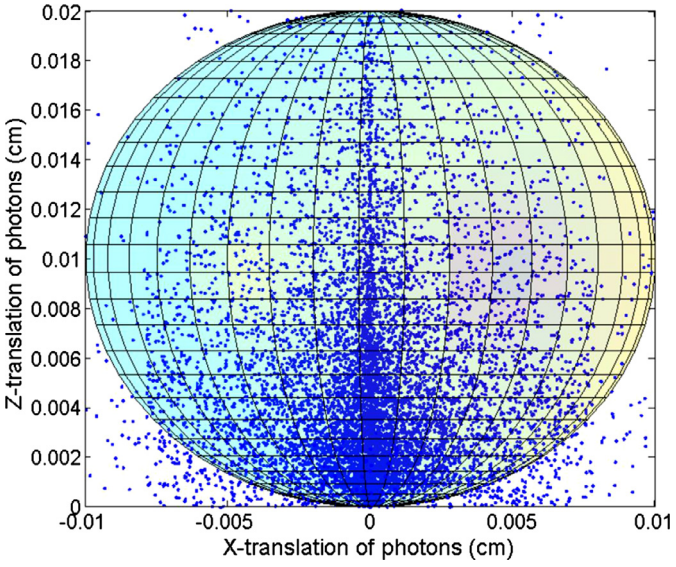

Fig. 17. Photon penetration into 3 wt.% 50 nm graphite in ethanol nanofluid droplet at $\lambda = 4300$ nm. The scatter represents final position of the photons inside the nanofluid.

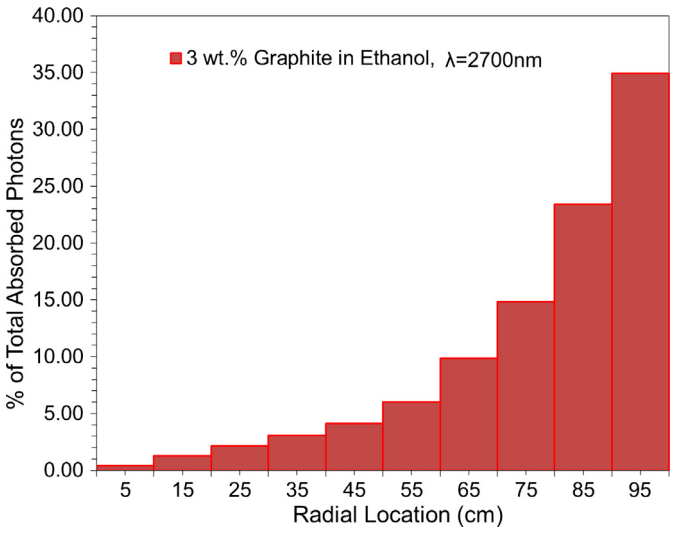

Fig. 18. The percentage of the total absorbed photons, starting at the center of the droplet toward the surface, as function of radial location for wavelength 2700 nm.

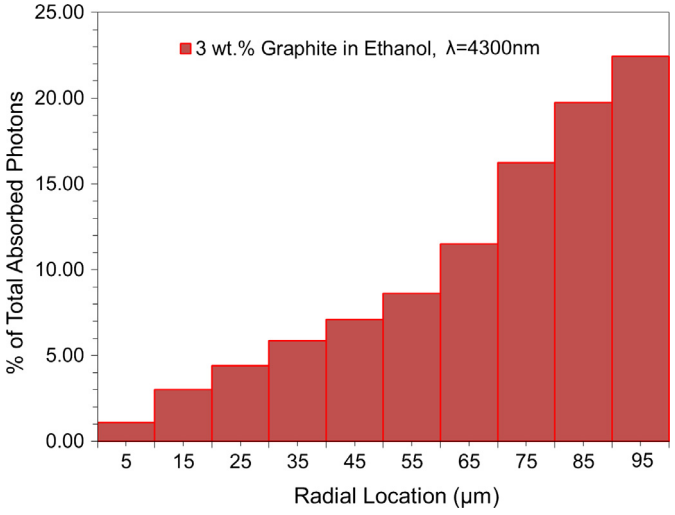

Fig. 19. The percentage of total absorbed photons, starting at the center of the droplet toward the surface, as function of radial location for wavelength 4300 nm.

same particle concentrations, the penetration depth of photons at $\lambda = 4300$ nm is more than that observed for the $\lambda = 2700$ nm case. This is again due to reduction in absorption coefficient as we move from $\lambda = 2700$ nm to $\lambda = 4300$ nm (Fig. 7). Scattering coefficients determined at these wavelengths are extremely low and much smaller than the absorption coefficients. Therefore, it can be concluded that the ratio of absorbed energy to the incident energy can be accurately determined by the Beer–Lambert Law.

We can clearly see that for graphite nanoparticles, $\lambda = 2700$ nm and $\lambda = 4300$ nm are not the ideal wavelengths of incident radiation that would provide optimal absorption characteristics. However, even at this off-performance radiation from the ethanol flame, we still observe the radiation localization along the surface of the nanofluid. To better understand the spatial distribution of the absorbed photons, we break the 200-μm droplet down into 10 radial shells of 10 μm thickness each. Figures 18 and 19 illustrate the percentage of total absorbed photons in each shell, from the center of the droplet toward its surface, as function of radial location for 3 wt.% particle concentration. The height of each column represents the percentage of total absorbed photons at the radial depth of each shell. We clearly see that for a smaller wavelength of 2700 nm, the percentage of photons absorbed close to the surface increases. For 2700 nm wavelength and 3 wt.% graphite nanoparticles, the resulting nanofluid absorbs 77% of the total incoming radiation between the droplet surface and a radial position of 70% of droplet radius.

This localization or concentration of energy with increasing particle loading is caused by the enhancement of both scattering and absorption coefficients of the entire nanofluid. The increase in scattering and absorption coefficients leads to smaller propagation displacements by the photons allowing the photon energy to be absorbed close to the launch site (droplet surface). Similarly, as the wavelength increases from 2700 nm to 4300 nm, the photons become less concentrated at the surface. This is again attributed to the changes in optical properties (scattering and absorption coefficients) with increasing wavelength. As wavelength increases, the scattering and absorption coefficients decrease. This allows for

deeper penetration into the droplet from the launch site (droplet surface).

The localization of radiation near the surface of the nanofluid droplet at higher concentrations creates regions of local hot spots around the nanofluid droplet surface. The localization of added radiation energy augmented by the conduction from the flame promotes localized boiling of ethanol. It is believed that this localized boiling at and near the surface of the nanofluid droplet promotes faster vaporization of liquid ethanol and is mainly responsible for droplet burning rate increase. The particle size does not significantly affect the optical properties (absorption and scattering coefficients) as seen in Fig. 9. Since the light propagation process via Monte Carlo simulation is highly dependent on the absorption and scattering coefficients, particle size has little effect on the penetration depth of the photons.

Based on the Monte Carlo simulations, we also examined the energy absorbed or retained by the droplet as a percentage of the total incoming radiation. Even though some photons do manage to escape the boundary of the droplet, they undergo multiple scattering and partial absorption at each of those scattering events before they reach the boundary and escape. Therefore, by summing all the fractions of radiation absorbed by the droplet from each photon, we can estimate the total fraction of absorbed radiation by the droplet. Results confirm that the percentage of the total radiation energy absorbed (absorptivity) increases as a function of particle concentration. Furthermore, the results are comparable to those obtained through Mie theory presented in Fig. 9. For example, 1 wt.% addition of graphite at either of the two wavelengths leads to over 90% absorption of the total incoming radiation. At 3 wt.% addition and at 2700 nm wavelength, both methods give a 99.9% absorptivity.

4. Conclusions

A droplet stream combustion experiment was developed to measure the burning rate of graphite based nanofluids. In order to examine the radiation absorption of nanofluids, the optical properties of such nanofluid fuels were determined using Mie theory. Additionally, Monte Carlo simulation was carried out to see how the absorbed incoming radiation is distributed within the graphite–ethanol nanofluid fuel. The following are the major conclusions of the study:

1. The flame structure was characterized by two-stage burning of the nanofluid fuel. SEM on nanoparticle residues collected from the flame as well as time scale analysis revealed that aggregation effects may not play a significant role in burning process.
2. The burning rate was observed to increase with increasing particle concentration. Burning rate also increase for decreasing particle size. Droplet size had little impact on burning rate enhancement. The maximum increase was observed at the maximum concentration considered, 3 wt.% 50 nm graphite case (62%).
3. Results from the radiation absorptivity model indicate that the nanofluids become excellent absorbers of incoming radiation with only a small addition of graphite nanoparticles. The absorptivity was found to increase with increasing droplet size and was found to be a strong function of incoming radiation wavelength.
4. A Monte Carlo routine was developed to study the distribution of absorbed flame radiation inside the nanofluid. Results indicate that as particle concentration is increased, the penetration depth of the photons decreases. Illustrating that, at higher concentrations, most of the photons are absorbed close to the nanofluid surface. This causes localized boiling of ethanol at the surface resulting in an increase in vaporization rate.

Future work is to determine the correlation between radiation absorption of nanofluid fuels to the burning rate quantitatively through detailed numerical simulations. Interactions between photons (radiation emitted from the flame) and the hybrid fluid (both nanoparticles and liquid) will be taken into account. The detailed numerical simulations will provide quantitative insights on how radiation absorption enhances the burning rate of nanofluid droplets.

Acknowledgment

This work has been supported by the National Science Foundation (NSF) under grant CBET-1134006.

References

[1] R.A. Yetter, G.A. Risha, S.F. Son, Metal particle combustion and nanotechnology, Proc. Combust. Inst. 32 (2009) 1819–1838.
[2] E.L. Dreizin, Metal-based reactive nanomaterials, Prog. Energy Combust. 35 (2) (2009) 141–167.
[3] B. Van Devener, J.P.L. Perez, J. Jankovich, S.L. Anderson, Oxide-free, catalyst-coated, fuel-soluble, air-stable boron nanopowder as combined combustion catalyst and high energy density fuel, Energy Fuel 23 (2009) 6111–6120.
[4] B. Van Devener, S.L. Anderson, Breakdown and combustion of JP-10 fuel catalyzed by nanoparticulate CeO_2 and Fe_2O_3, Energy Fuel 20 (5) (2006) 1886–1894.
[5] H. Tyagi, P.E. Phelan, R. Prasher, R. Peck, T. Lee, J.R. Pacheco, P. Arentzen, Increased hot-plate ignition probability for nanoparticle-laden diesel fuel, Nano Lett. 8 (5) (2008) 1410–1416.
[6] D. Jackson, R. Hanson, Application of an aerosol shock tube for the kinetic studies of *n*-dodecane/nano-aluminum slurries, in: 44th AIAA/ASME/SAE/ASEE Joint Propulsion Conference and Exhibit, Hartford, CT., 2008.
[7] C. Allen, G. Mittal, C.J. Sung, E. Toulson, T. Lee, An aerosol rapid compression machine for studying energetic-nanoparticle-enhanced combustion of liquid fuels, Proc. Combust. Inst. 33 (2011) 3367–3374.
[8] G. Young, Metallic nanoparticles as fuel additives in airbreathing combustion, University of Maryland, College Park, 2007 (Ph.D. thesis).
[9] G. Young, Effect of nanoparticle additives in airbreathing combustion, in: 14th AIAA/AHI Space Planes and Hypersonic Systems and Technologies Conference, Canberra, Australia, 2006.
[10] J.L. Sabourin, R.A. Yetter, B.W. Asay, J.M. Lloyd, V.E. Sanders, G.A. Risha, S.F. Son, Effect of nano-aluminum and fumed silica particles on deflagration and detonation of nitromethane, Propellants Explos. Pyrotechnol. 34 (5) (2009) 385–393.
[11] J.L. Sabourin, R.A. Yetter, V.S. Parimi, Exploring the effects of nanostructured particles on liquid nitromethane combustion, J. Propuls. Power 26 (5) (2010) 1006–1015.
[12] J.L. Sabourin, D.M. Dabbs, R.A. Yetter, F.L. Dryer, I.A. Aksay, Functionalized graphene sheet colloids for enhanced fuel/propellant combustion, ACS Nano 3 (12) (2009) 3945–3954.
[13] K.W. McCown III, E.L. Petersen, Effects of nano-scale additives on the linear burning rate of nitromethane, Combust. Flame 161 (7) (2014) 1935–1943.
[14] S. Tanvir, L. Qiao, Effect of addition of energetic nanoparticles on droplet-burning rate of liquid fuels, J. Propuls. Power 31 (1) (2015) 408–415.
[15] F. Takahashi, F.L. Dryer, F.A. Williams, Combustion behavior of free boron slurry droplets, Symp. (Int.) Combust. 21 (1986) 1983–1991.
[16] T. Sakai, M. Saito, Single-droplet combustion of coal slurry fuels, Combust. Flame 51 (1983) 141–154.
[17] C. Segal, W. Shyy, Energetic fuels for combustion applications, J. Energy Resour. 118 (3) (1996) 180–186.
[18] S.C. Wong, S.R. Turns, Disruptive burning of aluminum carbon slurry droplets, Combust. Sci. Technol. 66 (1–3) (1989) 75–92.
[19] V. Khullar, H. Tyagi, N. Hordy, T.P. Otanicar, Y. Hewakuruppu, P. Modi, R.A. Taylor, Harvesting solar thermal energy through nanofluid-based volumetric absorption systems, Int. J. Heat Mass Transfer 77 (2014) 377–384.
[20] A. Lenert, E.N. Wang, Optimization of nanofluid volumetric receivers for solar thermal energy conversion, Solar Energy 86 (1) (2012) 253–265.
[21] T.P. Otanicar, P.E. Phelan, R.S. Prasher, G. Rosengarten, R.A. Taylor, Nanofluid-based direct absorption solar collector, J. Renew. Sustain. Energy 2 (3) (2010).
[22] R. Saidur, T.C. Meng, Z. Said, M. Hasanuzzaman, A. Kamyar, Evaluation of the effect of nanofluid-based absorbers on direct solar collector, Int. J. Heat Mass Transfer 55 (21-22) (2012) 5899–5907.
[23] R.A. Taylor, P.E. Phelan, T.P. Otanicar, R. Adrian, R. Prasher, Nanofluid optical property characterization: towards efficient direct absorption solar collectors, Nanoscale Res. Lett. 6 (2011) 1–11.
[24] Y.A. Gan, L. Qiao, Optical properties and radiation-enhanced evaporation of nanofluid fuels containing carbon-based nanostructures, Energy Fuel 26 (7) (2012) 4224–4230.
[25] A. Gedanken, Using sonochemistry for the fabrication of nanomaterials, Ultrason. Sonochem. 11 (2) (2004) 47–55.

[26] Y.A. Gan, Y.S. Lim, L. Qiao, Combustion of nanofluid fuels with the addition of boron and iron particles at dilute and dense concentrations, Combust. Flame 159 (4) (2012) 1732–1740.
[27] Y.A. Gan, L. Qiao, Combustion characteristics of fuel droplets with addition of nano and micron-sized aluminum particles, Combust. Flame 158 (2) (2011) 354–368.
[28] J.S. Park, K.D. Kihm, H. Kim, G. Lim, S. Cheon, J.S. Lee, Wetting and evaporative aggregation of nanofluid droplets on CVD-synthesized hydrophobic graphene surfaces, Langmuir 30 (28) (2014) 8268–8275.
[29] A.B. Djurisic, E.H. Li, Optical properties of graphite, J. Appl. Phys. 85 (10) (1999) 7404–7410.
[30] C.F. Bohren, D.R. Huffman, Absorption and scattering of light by small particles, Wiley, 1983.
[31] Y. Zheng, R.S. Barlow, J.P. Gore, Measurements and calculations of spectral radiation intensities for turbulent non-premixed and partially premixed flames, J. Heat Transfer 125 (4) (2003) 678–686.
[32] N.J. Hogan, A.S. Urban, C. Ayala-Orozco, A. Pimpinelli, P. Nordlander, N.J. Halas, Nanoparticles heat through light localization, Nano Lett. 14 (8) (2014) 4640–4645.
[33] J.C. Ramella-Roman, S.A. Prahl, S.L. Jacques, Three Monte Carlo programs of polarized light transport into scattering media: part I, Opt. Express 13 (12) (2005) 4420–4438.
[34] B.J. Lee, K. Park, T. Walsh, L.N. Xu, Radiative heat transfer analysis in plasmonic nanofluids for direct solar thermal absorption, J. Solar Energy 134 (2) (2012) 1–6.
[35] L. Wang, S.L. Jacques, L. Zheng, MCML—Monte Carlo modeling of light transport in multi-layered tissues, Comput. Methods Prog. Biomed. 47 (2) (1995) 131–146.